Journal of Sound and Vibration (1998) **215**(1), 125–142
Article No. sv981620

NON-LINEAR DYNAMICS OF THE FOLLOWER-LOADED DOUBLE PENDULUM WITH ADDED SUPPORT-EXCITATION

J. S. JENSEN

Department of Solid Mechanics, Technical University of Denmark, DK-2800 *Lyngby, Denmark*

(*Received* 1 *October* 1997, *and in final form* 9 *March* 1998)

The partially follower-loaded elastic double pendulum subjected to excitation of the support, parallel to the straight upright pendulum position, is studied. The effect of small-amplitude off-resonant (high-frequency) excitation on the linear stability and non-linear behaviour of the pendulum, is examined. By use of the method of direct partition of motion (DPM) [1] (Blekhman, 1994, Vibrational Mechanics), the model equations are transformed into autonomous equations with the high-frequency excitation approximated by equivalent static forces. Linear stability analysis shows that the support-excitation has a stabilizing effect for most system parameters, but can also destabilize the upright pendulum position in certain situations. Local post- and pre-critical non-linear behaviour is analyzed by using centre manifold reduction and normal forms. Support-excitation is seen to change the bifurcational behaviour qualitatively: e.g., supercritical bifurcations may change to become subcritical. Chaotic behaviour of the pendulum is shown to exist for a wider range of system parameters and initial conditions with added support-excitation, compared to the case of a fixed support.

1. INTRODUCTION

Linear stability and non-linear behaviour of the partially follower-loaded elastic double pendulum is analyzed, when the support is subjected to small-amplitude off-resonant (high-frequency) excitation, parallel to the straight upright pendulum position. This work is an extension/supplement to the work of Thomsen [2], who studied linear stability and non-linear (including chaotic) behaviour of the same system with a fixed support.

Structures subjected to follower-type forces are often encountered in machine industry and in civil applications, e.g., turbo machinery and compressors subjected to fluid loading, pipes/tubes conveying fluid and bridges, antennas and panels experiencing wind loading. Follower forces are also found acting on aircraft wings, rockets and vertical take-off and landing aircrafts, all of which are subjected to the thrust from jet motors. These structures may lose the stability of the original design by dynamic instability (flutter) or by static instability (divergence), due to the action of the follower forces. Safe structures are designed and dimensioned to withstand the forces encountered, while retaining stability. Often, however, these structures, in addition to the follower forces, are affected by high-frequency excitation, e.g., coming from unbalanced rotating machinery or from the surroundings. The presence of high-frequency excitation may change the stability properties and also the non-linear dynamic behaviour of the structure. High-frequency excitation could therefore also be added with the specific purpose of changing the dynamic behaviour of the structure. A deep understanding of the interaction between forces of the

0022–460X/98/310125 + 18 $30.00/0

follower-type and high-frequency excitation is thus necessary and useful for structural design and is the motivation for this study.

A simple physical model of a follower-loaded structure is used in this study. Despite being a simple model, the elastic double-pendulum with a partial follower-load displays two of the basic instability mechanisms encountered in real engineering systems. The partial follower-load allows for modelling pure conservative loads, and thus for description of instabilities of the divergence type. The formulation also enables the modelling of non-conservative follower-loads, and thus also flutter-type instabilities. Therefore, this model serves well as a basic model to examine how high-frequency excitation will affect these mentioned instability mechanisms. The double pendulum can be seen as a two-degree-of-freedom discrete approximation of the corresponding fixed–free continuous beam model, a system also known as Beck's column. The behaviour of the continuous model is closely related to the behaviour of, e.g., an aircraft wing under the action of thrust from a jet motor, and recently the system has been subjected to experimental analysis by Sugiyama *et al*. [3]. For other experimental realization and examination of structures with follower forces; see e.g., the work by Herrmann *et al*. [4].

Stability of follower-loaded structures has been the subject of many investigations. Ziegler [5] considered the linear stability of a follower-loaded double pendulum, and Bolotin [6] thoroughly described dynamic and static instability mechanisms associated with follower-loaded structures in general. Herrmann and Jong [7] extended the work of Ziegler to include partially following loads. The first study of non-linear behaviour of the double pendulum, to the author's knowledge, was done by Roorda and Nemat-Nasser [8], where they showed, e.g., the existence of limit cycles. Since then, a large number of papers have been devoted to non-linear analysis of this and similar systems. References to these works can be found in reference [2].

This work differs from previous work done on follower-loaded structures in that the interaction between the follower forces and added off-resonant (high-frequency) support-excitation is investigated.

Work has been done previously on structures subjected to high-frequency excitation. The possible stabilizing effect on high-frequency excitation was pointed out by Kapitza [9]. Even for support-excitation of small amplitude (nearly invisible to the human eye), a hanging pendulum could be stabilized in the upright position, thus behaving as if an invisible static torque was acting upon it. This system, now often referred to as Kapitza's pendulum, has later been investigated by other authors using different methods of analysis [1, 10]. Blekhman and Malakhova [11] considered a system similar to Kapitza's pendulum. On the pendulum-rod, a washer, free to slide, was attached. In addition to stabilizing the pendulum in the upright position, the washer was stabilized at a position along the rod, as if an invisible force was acting against gravity. Similar action of vibrations has been reported by Thomsen [12], where a mass was shown to slide slowly along a vibrating string or beam, due to non-linear components of the vibrational force, and by Jensen [13, 14] where fluid or flexible material was driven inside a vibrating pipe also by the action of non-linear vibrational forces. Other interesting and sometimes even peculiar effects of high-frequency excitation can be found in reference [1].

The paper is organized as follows. In section 2 the model is presented and the model equations are derived. Section 3 provides a de-coupling between the fast and the slow motions in the system by using the method of Direct Partition of Motion (DPM). This yields a set of autonomous equations governing the essential system behaviour, approximating the effect of the support-excitation by equivalent static forces. The region of stability of the upright pendulum position is investigated in section 4, showing that added support-excitation mostly stabilizes the upright position, but for certain parameter

combinations can act destabilizing. In section 5, a local bifurcation analysis is performed using the methods of centre manifold reduction and normal forms. The analysis shows that the added support-excitation qualitatively changes the non-linear behaviour: e.g., by changing bifurcation types from supercritical to subcritical. In section 6, the global dynamic behaviour of the pendulum is analyzed numerically. Chaotic behaviour is seen to exist for a broader parameter range when the support is subjected to the high-frequency excitation, compared to the case of a fixed support.

2. THE MODEL AND MODEL EQUATIONS

Figure 1 shows the model. The system considered consists of two rigid massless rods of equal length l. The rods are connected to each other and to the support by hinges with equal linear torsional stiffness coefficient k and equal linear viscous damping coefficient $\tilde{c}$. The rods carry two masses $2m$ and m positioned at the end of the first and second rod, respectively. This mass distribution most closely corresponds to a continuos beam. The angles of the rods, in respect to the straight upright position, are given as θ_1 and θ_2. The system is subjected to a partially follower-load $\tilde{p}$ acting at the free rod end. The load arrangement is characterized by the parameter α, where $\alpha = 1$ corresponds to pure tangential loading and $\alpha = 0$ corresponds to pure conservative loading. The support is subjected to a harmonic displacement parallel to the upright position given as $\tilde{w} \sin \tilde{\Omega} t$, where $\tilde{w}$ is the amplitude and $\tilde{\Omega}$ the frequency of displacement. Small-amplitude, off-resonant (high-frequency) excitation is considered, implying that $\tilde{w} \ll l$ and $\tilde{\Omega} \gg \omega_2$, where ω_2 is the highest natural frequency of the pendulum.

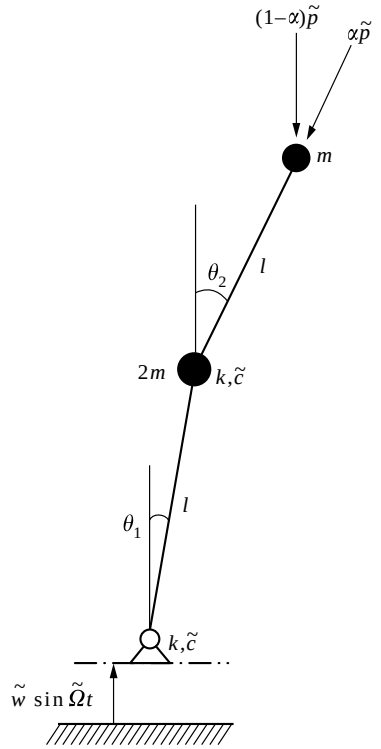

Figure 1. The elastic partially follower-loaded double pendulum with added support-excitation.

The kinetic energy T and the potential energy V of the system are given as, respectively,

$$T = \tfrac{3}{2}ml^2\dot{\theta}_1^2 + \tfrac{1}{2}ml^2(\dot{\theta}_2^2 + 2\dot{\theta}_1\dot{\theta}_2\cos(\theta_2 - \theta_1)) + \tfrac{3}{2}m\tilde{w}^2\tilde{\Omega}^2\cos^2\tilde{\Omega}t$$
$$- (3\dot{\theta}_1\sin\theta_1 + \dot{\theta}_2\sin\theta_2)ml\tilde{w}\tilde{\Omega}\cos\tilde{\Omega}t,$$
$$V = \tfrac{1}{2}k\theta_1^2 + \tfrac{1}{2}k(\theta_2 - \theta_1)^2, \qquad D = \tfrac{1}{2}\tilde{c}\dot{\theta}_1^2 + \tfrac{1}{2}\tilde{c}(\dot{\theta}_2 - \dot{\theta}_1)^2,$$
$$Q_1 = \tilde{p}l((1-\alpha)\sin\theta_1 - \alpha\sin(\theta_2 - \theta_1)), \qquad Q_2 = \tilde{p}l(1-\alpha)\sin\theta_2, \tag{1}$$

in which the viscous dissipation function D and the generalized forces Q_1 and Q_2 are given also.

The equations of motion are set up by using Lagrange's equations:

$$\frac{\mathrm{d}}{\mathrm{d}t}\frac{\partial(T-V)}{\partial\dot{\theta}_i} - \frac{\partial(T-V)}{\partial\theta_i} + \frac{\partial D}{\partial\dot{\theta}_i} = Q_i, \qquad i = 1, 2. \tag{2}$$

Applying Lagrange's equations using equation (1), leads to the two equations of motion:

$$3\ddot{\theta}_1 + (\cos(\theta_1 - \theta_2)\ddot{\theta}_2 + \sin(\theta_1 - \theta_2)\dot{\theta}_2^2) + 2c\dot{\theta}_1 - c\dot{\theta}_2 + 2\theta_1 - \theta_2$$
$$= p((1-\alpha)\sin\theta_1 + \alpha\sin(\theta_1 - \theta_2)) - 3w\Omega^2\sin\theta_1\sin\Omega\tau, \tag{3}$$
$$\ddot{\theta}_2 + (\cos(\theta_1 - \theta_2)\ddot{\theta}_1 - \sin(\theta_1 - \theta_2)\dot{\theta}_1^2) + c\dot{\theta}_2 - c\dot{\theta}_1 - \theta_1 + \theta_2$$
$$= p(1-\alpha)\sin\theta_2 - w\Omega^2\sin\theta_2\sin\Omega\tau, \tag{4}$$

where the following non-dimensional quantities have been introduced:

$$\tau \equiv \sqrt{\frac{k}{ml^2}}\,t, \qquad \Omega \equiv \sqrt{\frac{ml^2}{k}}\,\tilde{\Omega}, \qquad p \equiv \frac{\tilde{p}l}{k}, \qquad w \equiv \frac{\tilde{w}}{l}, \qquad c \equiv \frac{\tilde{c}}{\sqrt{kml^2}}. \tag{5}$$

3. DIRECT PARTITION OF MOTION

The model equations (3) and (4) contain parametric excitation terms. This makes stability analysis and non-linear analysis by using theoretical tools difficult. Also, with high-frequency excitation, numerical integration of the equations is time-consuming due to the necessity for small time-steps.

The method of direct partition of motion (DPM) [1], is used to eliminate the time-dependent terms in equations (3) and (4). DPM is an averaging technique, where the fast motion (comparable with the excitation frequency Ω) and the slow motion (comparable with the natural frequencies ω_i, $i = 1, 2$), are de-coupled. For this purpose the equations of motion are rewritten in the form, with $\boldsymbol{\theta} = \{\theta_1 \;\; \theta_2\}^T$,

$$\ddot{\boldsymbol{\theta}} = \mathbf{f}(\dot{\boldsymbol{\theta}}, \boldsymbol{\theta}) + \Omega\mathbf{q}(\boldsymbol{\theta}), \tag{6}$$

where

$$\mathbf{f}(\dot{\boldsymbol{\theta}}, \boldsymbol{\theta}) = \frac{1}{3 - \cos^2(\theta_1 - \theta_2)}\begin{Bmatrix} -\sin(\theta_1 - \theta_2)\dot{\theta}_2^2 - \tfrac{1}{2}\sin 2(\theta_1 - \theta_2)\dot{\theta}_1^2 - c(2\dot{\theta}_1 - \dot{\theta}_2) \\ \tfrac{1}{2}\sin 2(\theta_1 - \theta_2)\dot{\theta}_2^2 + 3\sin(\theta_1 - \theta_2)\dot{\theta}_1^2 + 3c(\dot{\theta}_1 - \dot{\theta}_2) \end{Bmatrix}$$
$$+ \begin{matrix} -c(\dot{\theta}_1 - \dot{\theta}_2)\cos(\theta_1 - \theta_2) - (2 + \cos(\theta_1 - \theta_2))\theta_1 + (1 + \cos(\theta_1 - \theta_2))\theta_2 \\ +c(2\dot{\theta}_1 - \dot{\theta}_2)\cos(\theta_1 - \theta_2) + (3 + 2\cos(\theta_1 - \theta_2))\theta_1 - (3 + \cos(\theta_1 - \theta_2))\theta_2 \end{matrix}$$
$$+ \begin{Bmatrix} +p((1-\alpha)\sin\theta_1 + \alpha\sin(\theta_1 - \theta_2)) - p(1-\alpha)\sin\theta_2\cos(\theta_1 - \theta_2) \\ -p((1-\alpha)\sin\theta_1 + \alpha\sin(\theta_1 - \theta_2))\cos(\theta_1 - \theta_2) + 3p(1-\alpha)\sin\theta_2 \end{Bmatrix}, \tag{7}$$

$$\mathbf{q}(\boldsymbol{\theta}) = \frac{w\Omega}{3 - \cos^2(\theta_1 - \theta_2)} \begin{Bmatrix} \sin\theta_2 \cos(\theta_1 - \theta_2) - 3\sin\theta_1 \\ 3\sin\theta_1 \cos(\theta_1 - \theta_2) - 3\sin\theta_2 \end{Bmatrix} \sin\Omega\tau. \tag{8}$$

In equation (6), terms with explicit dependence on $\Omega\tau$ have been collected in the vector $\mathbf{q} = \{q_1 \ q_2\}^T$, and the remaining terms have been collected in the vector $\mathbf{f} = \{f_1 \ f_2\}^T$.

Two independent time-scales are now introduced: a slow time scale $T_0 \equiv \tau$ and a fast time scale $T_1 \equiv \Omega\tau = \Omega T_0$. It is assumed that the solution to equation (6) can be written as a sum of a "slow" function $\mathbf{x}(T_0) = \{x_1(T_0)x_2(T_0)\}^T$ and a "fast" function $\boldsymbol{\psi}(T_1) = \{\psi_1(T_1)\psi_2(T_1)\}^T$. The assumed solution is written on the form

$$\boldsymbol{\theta}(T_0, T_1) = \mathbf{x}(T_0) + \varepsilon\boldsymbol{\psi}(T_1). \tag{9}$$

where $\varepsilon \equiv 1/\Omega (\varepsilon \ll 1)$ has been introduced. It is assumed that the fast function $\boldsymbol{\psi}(T_1)$ is a 2π-periodic function of T_1 with $\langle\boldsymbol{\psi}\rangle = 0$, where $\langle\ \rangle \equiv 1/2\pi \int_0^{2\pi} (\ )\mathrm{d}(T_1)$ is a linear averaging operator: i.e., averaging with respect to T_1 over 2π (a forcing period).

The solution assumption given in equation (9) is inserted into equation (6) to yield

$$D_0^2\mathbf{x} + \varepsilon^{-1}D_1^2\boldsymbol{\psi} = \mathbf{f}(D_0\mathbf{x} + D_1\boldsymbol{\psi}, \mathbf{x} + \varepsilon\boldsymbol{\psi}) + \varepsilon^{-1}\mathbf{q}(\mathbf{x} + \varepsilon\boldsymbol{\psi}), \tag{10}$$

where the notation $D_i^j \equiv \partial^j/\partial T_i^j$, denoting partial differentiation with respect to the individual time-scales, has been employed.

Applying the averaging operator to both sides of equation (10) yields

$$D_0^2\mathbf{x} = \langle\mathbf{f}(D_0\mathbf{x} + D_1\boldsymbol{\psi}, \mathbf{x} + \varepsilon\boldsymbol{\psi}) + \varepsilon^{-1}\mathbf{q}(\mathbf{x} + \varepsilon\boldsymbol{\psi})\rangle, \tag{11}$$

where the following properties of the averaging operator have been used: $\langle D_0^2\mathbf{x}\rangle = D_0^2\mathbf{x}$ and $\langle D_1^2\boldsymbol{\psi}\rangle = 0$. Equation (11) is then subtracted from equation (10) to yield

$$\begin{aligned} D_1^2\boldsymbol{\psi} = {} & \varepsilon\mathbf{f}(D_0\mathbf{x} + D_1\boldsymbol{\psi}, \mathbf{x} + \varepsilon\boldsymbol{\psi}) + \mathbf{q}(\mathbf{x} + \varepsilon\boldsymbol{\psi}) \\ & - \langle\varepsilon\mathbf{f}(D_0\mathbf{x} + D_1\boldsymbol{\psi}, \mathbf{x} + \varepsilon\boldsymbol{\psi}) + \mathbf{q}(\mathbf{x} + \varepsilon\boldsymbol{\psi})\rangle. \end{aligned} \tag{12}$$

Applying the first-order Taylor expansion: $\mathbf{q}(\mathbf{x} + \varepsilon\boldsymbol{\psi}) \approx \mathbf{q}(\mathbf{x}) + \varepsilon\boldsymbol{\psi} \cdot \partial\mathbf{q}(\mathbf{x})/\partial\mathbf{x}$, yields

$$D_0^2\mathbf{x} = \langle\mathbf{f}(D_0\mathbf{x} + D_1\boldsymbol{\psi}, \mathbf{x} + \varepsilon\boldsymbol{\psi}) + \varepsilon^{-1}\mathbf{q}(\mathbf{x}) + \boldsymbol{\psi} \cdot \partial\mathbf{q}(\mathbf{x})/\partial\mathbf{x}\rangle, \tag{13}$$

$$\begin{aligned} D_1^2\boldsymbol{\psi} = {} & \varepsilon\mathbf{f}(D_0\mathbf{x} + D_1\boldsymbol{\psi}, \mathbf{x} + \varepsilon\boldsymbol{\psi}) + \mathbf{q}(\mathbf{x}) + \varepsilon\boldsymbol{\psi} \cdot \partial\mathbf{q}(\mathbf{x})/\partial\mathbf{x} \\ & - \langle\varepsilon\mathbf{f}(D_0\mathbf{x} + D_1\boldsymbol{\psi}, \mathbf{x} + \varepsilon\boldsymbol{\psi}) + \mathbf{q}(\mathbf{x}) + \varepsilon\boldsymbol{\psi} \cdot \partial\mathbf{q}(\mathbf{x})/\partial\mathbf{x}\rangle. \end{aligned} \tag{14}$$

The zero-order approximation: $\mathbf{f}(D_0\mathbf{x} + D_1\boldsymbol{\psi}, \mathbf{x} + \varepsilon\boldsymbol{\psi}) \approx \mathbf{f}(D_0\mathbf{x} + D_1\boldsymbol{\psi}, \mathbf{x})$ is now applied, giving terms with accuracy up to the desired ε^0 in equation (13) and up to ε^1 in equation (14). Using also $\langle\mathbf{q}(\mathbf{x})\rangle = 0$, yields the following two equations:

$$D_0^2\mathbf{x} = \langle\mathbf{f}(D_0\mathbf{x} + D_1\boldsymbol{\psi}, \mathbf{x}) + \boldsymbol{\psi} \cdot \partial\mathbf{q}(\mathbf{x})/\partial\mathbf{x}\rangle, \tag{15}$$

$$D_1^2\boldsymbol{\psi} = \mathbf{q}(\mathbf{x}) + \varepsilon[\mathbf{f}(D_0\mathbf{x} + D_1\boldsymbol{\psi}, \mathbf{x}) + \boldsymbol{\psi} \cdot \partial\mathbf{q}(\mathbf{x})/\partial\mathbf{x} - \langle\mathbf{f}(D_0\mathbf{x} + D_1\boldsymbol{\psi}, \mathbf{x}) + \boldsymbol{\psi} \cdot \partial\mathbf{q}(\mathbf{x})/\partial\mathbf{x}\rangle]. \tag{16}$$

Equations (15) and (16) constitute a coupled set of differential equations, representing an alternative formulation of equation (6) with the assumption that the solution can be written on the form given in equation (9), and under the additional assumptions made in the previous derivation.

To solve the new equations, a zero-order approximation of equation (16), $D_1^2\boldsymbol{\psi} \approx \mathbf{q}(\mathbf{x})$, is used, which gives terms of the desired accuracy ϵ^0 when substituted back into equation (15). Solving equation (16) for $\boldsymbol{\psi}$ yields

$$\boldsymbol{\psi} = \frac{-w\Omega}{3 - \cos^2(x_1 - x_2)} \begin{Bmatrix} \sin x_2 \cos(x_1 - x_2) - 3 \sin x_1 \\ 3 \sin x_1 \cos(x_1 - x_2) - 3 \sin x_2 \end{Bmatrix} \sin T_1. \tag{17}$$

Solving equation (15), using equation (17), and writing the obtained solution in the same form as equations (3) and (4), yields the two equations governing the slow motion of the system:

$$\begin{aligned} 3\ddot{x}_1 + (\cos(x_2 - x_1)\ddot{x}_2 - \sin(x_2 - x_1)\dot{x}_2^2) + c(2\dot{x}_1 - \dot{x}_2) + 2x_1 - x_2 \\ = p((1 - \alpha)\sin x_1 - \alpha \sin(x_2 - x_1)) + V_1, \end{aligned} \tag{18}$$

$$\ddot{x}_2 + (\cos(x_2 - x_1)\ddot{x}_1 + \sin(x_2 - x_1)\dot{x}_1^2) + c(\dot{x}_2 - \dot{x}_1) - x_1 + x_2 = p(1 - \alpha)\sin x_2 + V_2. \tag{19}$$

Here

$$\begin{Bmatrix} V_1 \\ V_2 \end{Bmatrix} = \frac{v}{(\cos(2x_1 - 2x_2) - 5)^3} \begin{Bmatrix} 102 \sin 2x_1 - 2 \sin(2x_1 - 4x_2) \\ \sin(2x_1 - 4x_2) + \sin(6x_1 - x_2) \end{Bmatrix}$$

$$+ \begin{Bmatrix} -10 \sin(4x_1 - 2x_2) + 20 \sin(2x_1 - 2x_2) - 2 \sin(4x_1 - 4x_2) - 30 \sin 2x_2 \\ -10 \sin(4x_1 - 2x_2) - 20 \sin(2x_1 - 2x_2) + 2 \sin(4x_1 - 4x_2) + 10 \sin 2x_2 \end{Bmatrix}, \tag{20}$$

with

$$v \equiv \tfrac{3}{4}(w\Omega)^2, \tag{21}$$

introduced as a measure of the vibrational force (the factor $\frac{3}{4}$ is chosen merely for convience).

The two functions V_i, $i = 1, 2$, represent the vibrational forcing acting on the slow motion of the system, i.e., motion comparable to the natural frequencies of the pendulum, as a result of the high-frequency support-excitation. Note that by means of DPM the explicit time-dependence has been eliminated in the new model equations (18) and (19). The effect of the high-frequency excitation is instead approximated by equivalent static forces. Except for V_i, equations (18) and (19) are identical to those found in, e.g., reference [2], where the support was fixed.

4. LINEAR STABILITY OF THE UPRIGHT PENDULUM POSITION

From equations (18)–(20) it is noted that $\{x_1 x_2\}^T = \{0 \;\; 0\}^T$ is a solution, also with added support-excitation. In this section, the effect of the support-excitation on the linear stability of this solution, i.e., the straight upright pendulum position, is investigated.

Linearizing equations (18) and (19) around $\{x_1 x_2\}^T = \{0 \;\; 0\}^T$ and writing the equations as a system of four first order differential equations, using the notation $\mathbf{y} = \{x_1 \;\; x_2 \;\; \dot{x}_1 \;\; \dot{x}_2\}^T$, yields

$$\dot{\mathbf{y}} = \mathbf{A}\mathbf{y}, \tag{22}$$

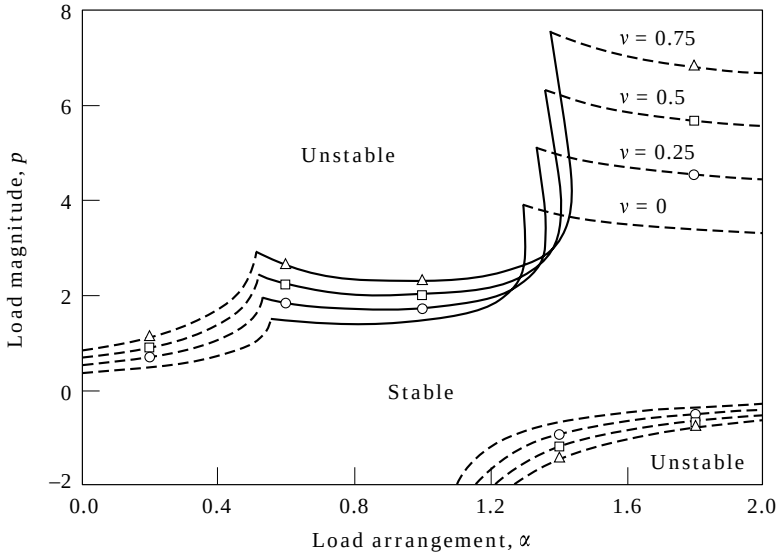

Figure 2. Stability borders for the straight upright pendulum position, computed by use of equations (27) and (28), for four different amounts of support-excitation. Solid lines: Hopf bifurcations; dashed lines: pitchfork bifurcations; markers: stability borders calculated by numerical integration. Parameter values: $c = 0{\cdot}1$, $\Omega = 25$.

where

$$\mathbf{A} = \begin{bmatrix} \mathbf{0} & \mathbf{I} \\ -\mathbf{M}^{-1}\mathbf{K} & -\mathbf{M}^{-1}\mathbf{C} \end{bmatrix}, \tag{23}$$

with $\mathbf{0}$ and $\mathbf{I}$ being the null and identity matrix respectively, and

$$\mathbf{M} = \begin{bmatrix} 3 & 1 \\ 1 & 1 \end{bmatrix}, \qquad \mathbf{C} = \begin{bmatrix} 2c & -c \\ -c & c \end{bmatrix}, \qquad \mathbf{K} = \begin{bmatrix} 2 - p + 3v & \alpha p - 1 - v \\ -1 - v & 1 - p(1-\alpha) + v \end{bmatrix}. \tag{24}$$

Upon inspecting the stiffness matrix $\mathbf{K}$, it is noted that the presence of support-excitation acts, for small angles, approximately as additional springs.

Exponential time-dependence of the form $\mathbf{y} = \mathbf{u}\exp(\lambda\tau)$ is now assumed, and inserted into equation (22). Solving the determinant equation $\det(\mathbf{A} - \lambda\mathbf{I}) = 0$, yields the characteristic equation for the eigenvalue λ,

$$a_0\lambda^4 + a_1\lambda^3 + a_2\lambda^2 + a_3\lambda + a_4 = 0, \tag{25}$$

where

$$a_0 = 2, \quad a_1 = 7c, \quad a_2 = 2p(\alpha - 2) + c^2 + 7 + 8v,$$
$$a_3 = c(3p(\alpha - 1) + 2 + 3v), \quad a_4 = (3 - p + 4v)p(\alpha - 1) + (2v + 1)(v + 1). \tag{26}$$

The zero solution of equation (22) is stable only if all roots of λ in equation (25) have negative real parts. The zero solution will lose stability by a static instability, known as divergence, if a single real eigenvalue passes the origin. The condition for this is [15]

$$a_4 = 0. \tag{27}$$

The condition for a dynamic instability, i.e., if a pair of complex conjugate eigenvalues passes the imaginary axis, also known as a flutter instability, becomes [15]

$$a_1 a_2 a_3 - a_4 a_1^2 - a_0 a_3^2 = 0, \quad a_3 / a_1 > 0. \tag{28}$$

Figure 2 shows the regions of stability of the upright pendulum position in an (α, p) co-ordinate-system, for four different values of the vibrational forcing parameter v. It is also indicated whether stability of the upright position is lost by divergence (dashed lines) or by flutter (solid lines). More detailed stability diagrams can be found in references [2, 7] for the system without added support-excitation.

With vibrational forcing ($v \neq 0$) added, the region of linear stability is broadened. Stability borders are moved up (down) for $p > 0$ ($p < 0$) respectively, especially for the upper right divergence region, found for $\alpha > \approx 1{\cdot}4$, $p > 0$. In this region, the stability of the upright position is improved significantly with the added support-excitation. However, as an exception, around $\alpha = 1{\cdot}3$ the presence of vibrational forcing may destabilize the pendulum. The stability border for flutter moves to the right for growing values of v. This implies that loads which previously did not affect the upright position, may now cause the pendulum to flutter (see also Figure 3).

The markers in Figure 2 represent stability borders computed by numerical integration of the full model equations (3) and (4), using a standard Runge–Kutta algorithm. Very good agreement is noted, indicating that DPM accurately captures the full effect of the support-excitation in respect to linear stability.

Figure 3 shows time-series displaying how added support-excitation can both stabilize and destabilize the upright pendulum position. Transient behaviour of the lower rod angle θ_1 is shown, both for zero vibrational forcing ($v = 0$), shown as dashed lines, and for $v = 0{\cdot}5$, shown as solid lines. For $p = 2$ and $\alpha = 1{\cdot}2$ (Figure 3(a)), the initially applied disturbance is amplified for $v = 0$, whereas with support-excitation present the vibrations are damped out to approach the stable zero solution. For another set of load parameters, $(\alpha, p) = (1{\cdot}32, 3)$ (Figure 3(b)), the upright position is stable for the stationary pendulum, whereas when support-excitation is added, the zero solution is destabilized. This causes the initial disturbance of the pendulum to be amplified, until the motion is finally limited by stabilizing non-linear terms (see also section 5). In Figure 3 it is noted that the frequency of vibrations is increased when the vibrational forcing is added. This feature is common in systems subjected to high-frequency excitation, [1].

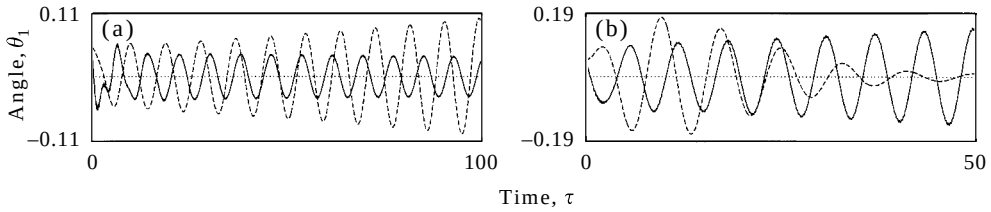

Figure 3. Lower rod angle θ_1 versus time τ, based on numerical integration of equations (3) and (4). Solid lines: $v = 0{\cdot}5$; dashed lines: $v = 0$; (a) $p = 2$, $\alpha = 1{\cdot}2$; (b) $p = 3$, $\alpha = 1{\cdot}32$. Parameter values: $c = 0{\cdot}1$, $\Omega = 25$. Initial conditions $(0{\cdot}05, -0{\cdot}07, 0, 0)$.

5. LOCAL PERIODIC AND NON-ZERO STATIC SOLUTIONS

Local bifurcations of the zero solution are now investigated by using the methods of centre manifold reduction and normal forms. Only behaviour associated with simple bifurcations (codimension one), i.e., either pure flutter or pure divergence, is analyzed. Codimension two bifurcations, i.e., coupled flutter and divergence, is beyond the scope of this paper. Emphasis is put on the qualitative effect of the added support-excitation on the bifurcation types: i.e., whether the bifurcations are super- or subcritical. Subcritical bifurcations are of primary interest, since, even when the upright pendulum position is linearly stable, i.e., stable to small disturbances, a stronger disturbance may destabilize this position.

Taylor expanding non-linear terms in equations (18) and (19) near the zero solution $\{y_1 \ y_2\}^T = \{0 \ 0\}^T$, and truncating the expansion for $y_i^p y_j^q y_k^r$, $i, j, k = 1, \ldots, 4$, $p + q + r > 3$, yields a system of four first order differential equations,

$$\dot{\mathbf{y}} = \mathbf{A}\mathbf{y} + \mathbf{f}(\mathbf{y}), \tag{29}$$

where $\mathbf{f}$ is a vector containing cubical non-linearities, given as

$$\mathbf{f}(\mathbf{y}) = \sum_{j,k,l=1}^{4} \mathbf{b}_{jkl} y_j y_k y_l, \tag{30}$$

with the non-zero components of the vectors $\mathbf{b}$ given in the Appendix.

Equation (29) is now written in Jordan canonical form, by using the co-ordinate transformation $\mathbf{y} = \mathbf{P}\mathbf{z}$ with $\mathbf{z} = \{z_1 \ z_2 \ z_3 \ z_4\}^T$, yielding

$$\dot{\mathbf{z}} = \mathbf{\Lambda}\mathbf{z} + \mathbf{g}(\mathbf{z}), \tag{31}$$

where $\mathbf{\Lambda} = \mathbf{P}^{-1}\mathbf{A}\mathbf{P}$ and $\mathbf{g}(\mathbf{z}) = \mathbf{P}^{-1}\mathbf{f}(\mathbf{P}\mathbf{z})$, and $\mathbf{P}$ is the so-called modal matrix composed of imaginary and real parts of the eigenvectors; see, e.g., reference [16]. The matrix $\mathbf{\Lambda}$ takes the form

$$\mathbf{\Lambda} = \begin{bmatrix} \mathbf{\Lambda}_{cri} & \mathbf{0} \\ \mathbf{0} & \mathbf{\Lambda}_{stable} \end{bmatrix}. \tag{32}$$

The matrix $\mathbf{\Lambda}$ is in block form which allows for a de-coupling of the linear part of equation (31) into an essential part $\mathbf{\Lambda}_{cri}$ associated with the critical eigenvalues (the ones with zero real part) and a stable part $\mathbf{\Lambda}_{stable}$ associated with eigenvalues with negative real parts. With a subsequent de-coupling of the non-linear function $\mathbf{g}$ (known as the centre manifold reduction), the essential system behaviour can be traced on a lower dimensional sub-system. For further details see, e.g., references [17, 18]. Further simplification of the system can then be made by using normal forms; see, e.g. reference [19]. In the following Hopf- and pitchfork-bifurcations will be studied separately in a non-detailed manner. For further details on the application of the methods of centre manifold reduction and normal forms in similar systems see, e.g., references [20, 21].

5.1. HOPF BIFURCATIONS

The non-linear dynamics associated with a Hopf bifurcation can be analyzed by examining the two-dimensional sub-system given as, with $\mathbf{z}_{cri} = \{z_1 \ z_2\}^T$, $\mathbf{g}_{cri}(\mathbf{z}) = \{g_1(\mathbf{z}) \ g_2(\mathbf{z})\}^T$,

$$\dot{\mathbf{z}}_{cri} = \begin{bmatrix} \kappa & -\omega \\ \omega & \kappa \end{bmatrix} \mathbf{z}_{cri} + \mathbf{g}_{cri}(\mathbf{z}), \tag{33}$$

where ω and κ are the imaginary and real parts of the critical eigenvalue. At the critical point ω represents the flutter frequency whereas κ vanishes.

The two scalar non-linear functions g_1 and g_2 are still coupled to the remaining (stable) system. As in references [20, 21], the tangent-space approximation $\mathbf{g}_{cri}(\mathbf{z}) \approx \mathbf{g}_{cri}(\mathbf{z}_{cri}, \mathbf{0})$ can be applied with no additional approximations introduced. This leads to the following set of equations:

$$\dot{z}_1 = \kappa z_1 - \omega z_2 + g_1(z_1, z_2), \tag{34}$$

$$\dot{z}_2 = \omega z_1 + \kappa z_2 + g_2(z_1, z_2). \tag{35}$$

Equations (34) and (35) are now to be simplified by using the method of normal forms. Since the behaviour near the bifurcation point is of interest, the chosen outfolding parameter, e.g., the load magnitude p, is perturbed so that $p = p_{cri} + \delta$. From the perturbation parameter δ, the changes in the real and imaginary parts of the eigenalue δ_1 and δ_2 can be computed (see, e.g., references [20, 21]): i.e., for a given perturbation,

$$\kappa \to 0 + \delta_1, \qquad \omega \to \omega + \delta_2. \tag{36}$$

With the expressions (36) inserted and the functions g_1 and g_2 written out, equations (34) and (35) then become

$$\dot{z}_1 = \delta_1 z_1 - (\omega + \delta_2) z_2 + a_1 z_1^3 + a_2 z_1^2 z_2 + a_3 z_1 z_2^2 + a_4 z_2^3, \tag{37}$$

$$\dot{z}_2 = (\omega + \delta_2) z_1 + \delta_1 z_2 + a_5 z_1^3 + a_6 z_1^2 z_2 + a_7 z_1 z_2^2 + a_8 z_2^3. \tag{38}$$

The constants a_i, $i = 1, \ldots, 8$, depend on the system parameters. They are lengthy and are not shown.

By using the polar co-ordinate transformation $z_1 = r \cos \phi$ and $z_2 = r \sin \phi$, the normal form of equations (37) and (38) becomes [19]

$$\dot{r} = r(\delta_1 + a r^2), \qquad \dot{\phi} = \omega + \delta_2 + b r^2, \tag{39, 40}$$

where $a = \frac{1}{8}(3a_1 + a_3 + a_6 + 3a_8)$ and $b = -\frac{1}{8}(a_2 + 3a_4 - 3a_5 - a_7)$. In equations (39) and (40), r governs the amplitude of oscillations, whereas ϕ is the phase angle.

Steady state values of r are found by letting $\dot{r} = 0$ in equation (39). Two solutions for r ($r \geqslant 0$) are found,

$$r = 0, \qquad r = \sqrt{-\delta_1/a} \quad \text{for} \quad \delta_1/a < 0: \tag{41}$$

that is, the zero solution and a non-linear limit cycle solution. With known oscillation amplitude r, equation (40) can be solved for the steady state phase angle velocity $\dot{\phi}$. The obtained solution can then, if desired, be transformed back to be expressed in terms of the original variable $\mathbf{y}$.

Here the type of bifurcation is of main interest. This can be determined solely from the constant a. For $a < 0$, equation (39) predicts a supercritical Hopf bifurcation whereas $a > 0$ corresponds to a subcritical bifurcation. The value of a turns out to depend strongly

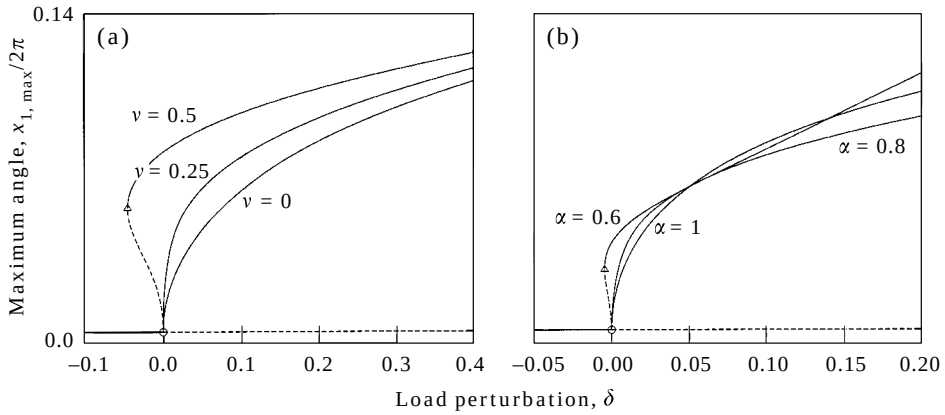

Figure 4. Maximum lower rod angle $x_{1,max}/2\pi$ versus load perturbation δ for flutter instabilities, based on numerical integration of equations (18) and (19) using PATH; (a) $\alpha = 0{\cdot}8$ for three different values of v; and (b) $v = 0{\cdot}25$ for three different values of α. Solid and dashed lines: stable and unstable solutions, respectively. Hopf bifurcation: $\bigcirc$; saddle-node bifurcation: $\triangle$. Parameter values: $c = 0{\cdot}1$, $\Omega = 25$.

upon the amount of added support-excitation. If v is increased, a increases also, implying that the added support-excitation might turn supercritical Hopf bifurcations into subcritical ones.

For $\alpha = 0{\cdot}8$, i.e., rather close to a perfectly follower-loaded system, the bifurcation is supercritical without added support-excitation. However, the value of a is computed to turn from negative to positive for $v_{trans} \cong 0{\cdot}318$, and thus subcritical bifurcations are predicted for values of v higher than this value. Figure 4(a) shows limit cycle solutions obtained with the algorithm PATH [22], based on numerical integration of the autonomous model equations (18) and (19). PATH is a path-following algorithm capable of following stable and unstable solution branches. Hopf bifurcations of the zero solution are shown for three different values of the vibrational forcing parameter v. Figure 4(a) shows supercritical bifurcations for the two lower values of v, and a subcritical bifurcation of $v = 0{\cdot}5$, as predicted by the theoretical analysis. Figure 4(b) shows three Hopf bifurcations of the zero solution for $v = 0{\cdot}25$, for three different values of α. The theoretical value of a in this case increases for decreasing values of α, and is computed turn negative for $\alpha_{trans} \approx 0{\cdot}686$. It is seen that for $\alpha = 1$ and $\alpha = 0{\cdot}8$, the corresponding Hopf bifurcations are supercritical, whereas for $\alpha = 0{\cdot}6$ the bifurcation has turned subcritical, as predicted by theory.

Thus, the results presented in this section show that, with sufficiently strong support-excitation, the upright pendulum position may be destabilized in favour of flutter oscillations by a strong disturbance, even though the upright position is linearly stable. It should be noted also that secondary saddle-node bifurcations occur in the subcritical cases. These secondary bifurcations are not predicted by equation (41), which is based on a third order non-linear model, but is captured by PATH. To identify these bifurcations theoretically, higher order approximations are called for.

5.2. PITCHFORK BIFURCATIONS

The non-linear behaviour associated with pitchfork bifurcations is now analyzed. The essential behaviour is governed by the critical one-dimensional sub-system given as

$$\dot{\mathbf{z}}_{cri} = \kappa \mathbf{z}_{cri} + \mathbf{g}_{cri}(\mathbf{z}), \tag{42}$$

with $\mathbf{z}_{cri} = \{z\}$, $\mathbf{g}_{cri} = \{g(\mathbf{z})\}$, and where the real part of the eigenvalue κ, vanishes at the critical point. The decoupling of the non-linear function $\mathbf{g}_{cri}(\mathbf{z})$ is, analogously to section 5.1, performed as $\mathbf{g}_{cri}(\mathbf{z}) \approx \mathbf{g}_{cri}(\mathbf{z}_{cri}, \mathbf{0})$, without any additional approximations introduced. The non-linear behaviour is thus governed by the single scalar equation

$$\dot{z} = \delta_1 z + az^3, \tag{43}$$

where the change in the real part of the eigenvalue δ_1 is computed from a chosen perturbation parameter δ, and a is a lengthy constant that depends on the system parameters.

The steady state solution for z is found directly from equation (43) by letting $\dot{z} = 0$. This yields

$$z = 0, \qquad z = \pm\sqrt{-\delta_1/a} \quad \text{for} \quad \delta_1/a < 0: \tag{44}$$

that is, the zero solution and two static non-zero solution branches. As in section 5.1, $a < 0$ implies a supercritical bifurcation, whereas $a > 0$ corresponds to a subcritical bifurcation. Also in this case the value of a depends strongly upon the amount of support-excitation: i.e., the value of v.

Bifurcation types corresponding to the lower divergence region of Figure 2, i.e., for $\alpha > \approx 1{\cdot}1$ and $p < 0$, are illustrated by use of PATH, for different amounts of support-excitation and for different values of α. Figure 5(a) shows pitchfork bifurcations for $\alpha = 1{\cdot}7$, for three different values of v. Only positive values of $x_1/2\pi$ are shown since the curves are symmetrical around the abscissa. The transition from supercritical to subcritical, i.e., a turning positive, is computed to occur for $v_{trans} \approx 0{\cdot}255$. This agrees with what is shown in Figure 5(a). For $v = 0$ and $v = 0{\cdot}25$ the bifurcations are supercritical and for $v = 0{\cdot}5$, PATH shows a subcritical bifurcation. For $v = 0{\cdot}25$, the transition from super- to subcritical is predicted to occur for $\alpha_{trans} \approx 1{\cdot}600$ for decreasing α. The bifurcation curves in Figure 5(b), computed by use of PATH, show a supercritical bifurcation for $\alpha = 1{\cdot}7$, and for $\alpha = 1{\cdot}5$ (and $\alpha = 1{\cdot}3$), as predicted, subcritical ones.

Thus, also for divergence instabilities, the added support-excitation may turn bifurcations subcritical: i.e., even with the pendulum being linearly stable, a sufficiently strong disturbance may cause the pendulum to occupy another static point of equilibrium.

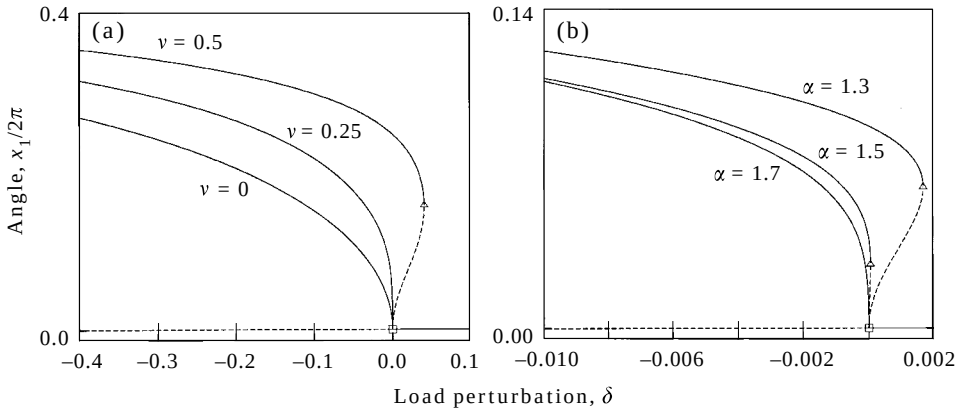

Figure 5. Lower rod angle $x_1/2\pi$ versus load perturbation δ, for divergence instabilities, based on numerical integration of equations (18) and (19) using PATH, (a) $\alpha = 1{\cdot}7$ for three different vlaues of v; and (b) $v = 0{\cdot}25$ for three different values of α. Solid and dashed lines: stable and unstable solutions, respectively. Pitchfork bifurcation: $\square$; saddle-node bifurcation: $\triangle$. Parameter values: $c = 0{\cdot}1$, $\Omega = 25$.

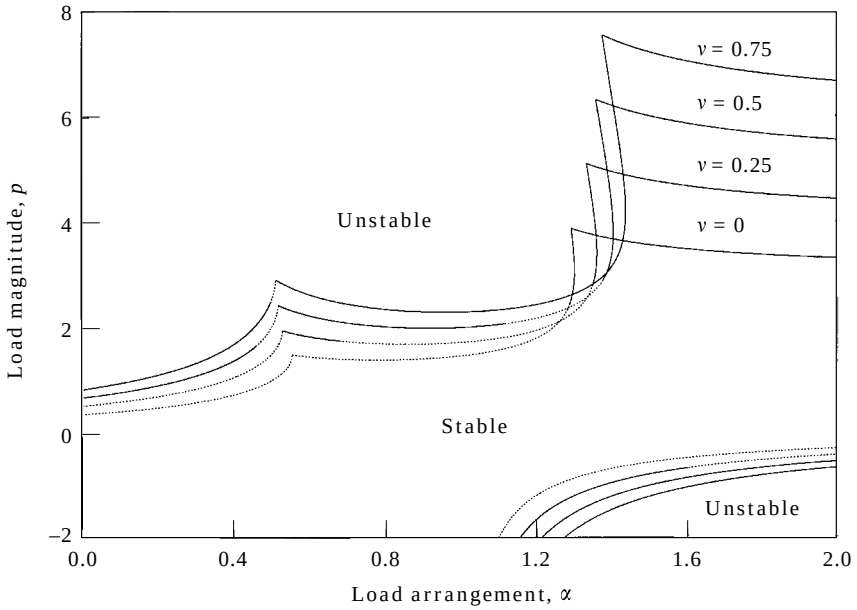

Figure 6. Local bifurcation diagram. Solid lines: subcritical bifurcations; dotted lines: supercritical bifurcations. Parameter values: $c = 0{\cdot}1$, $\Omega = 25$.

5.3. LOCAL BIFURCATION DIAGRAM

Sections 5.1 and 5.2 provided means for determining the type of bifurcation, i.e., either supercritical or subcritical, of the upright pendulum position in case of linear instability. Both the cases of Hopf birfurcations (flutter) and pitchfork bifurcations (divergence) were treated.

The stability diagram (Figure 2) presented in section 4 is now redrawn with special attention given to the type of bifurcations. Figure 6 shows this bifurcation diagram. Supercritical bifurcations are represented by dotted lines, whereas solid lines represent bifurcations of the subcritical kind. As in Figure 2, the bifurcation curves are shown for the case of no support-excitation and for three non-zero values of the parameter v.

For $v = 0$, supercritical bifurcations are seen to exist for most load arrangements. However, for the upper right divergence region, as well as for a small section of the flutter curve near the right codimension two point, the corresponding bifurcations are subcritical. When support-excitation is added, parts of the supercritical bifurcations turn into subcritical. This happens both for the flutter and for the divergence curves. With $v = 0{\cdot}75$ almost all bifurcations shown in Figure 6 are subcritical, except for a small part of the upper left divergence region near the left codimension two points. Also for higher values of v this small supercritical region prevails, with decreasing size however. It should be remembered though, that near codimension two points even more complicated dynamics may exist. As previously mentioned, this is not covered in this work. The transitions between bifurcation types, as shown in Figure 6, have been verified by PATH, as exemplified in sections 5.1 and 5.2, as well as by numerical integration of the original model equations.

Thus, the local bifurcation investigation has revealed that added support-excitation tends to turn supercritical bifurcations into subcritical ones. This has shown to occur both for divergence and for flutter instabilities.

6. GLOBAL DYNAMIC BEHAVIOUR

In section 5, local bifurcations were studied, and consequently the system behaviour near the straight upright pendulum position. In this section, the effect of the added support-excitation on the global dynamics of the pendulum, is studied. Special attention is given to regions in the (α, p) co-ordinate-system with chaotic dynamics.

Two regions with possible chaotic dynamics are investigated in detail. First, the behaviour of the pendulum with a pure tangential load, i.e., $\alpha = 1$, is studied. Then the system is analyzed for the case of $\alpha = 2$. The two cases correspond to a free system and a system hanging in gravity, respectively, under the action of a follower-force. In the analysis, the maximum Lyapunov exponent λ_1 is used as a characteristic variable. The values for λ_1 are computed by using the algorithm described by Wolf *et al*. [23], based on numerical integration of the full model equations (3) and (4). Also, phase-plots are shown, based on numerical integration of the autonomous set of equations (18) and (19).

6.1. PURE TANGENTIAL LOAD ($\alpha = 1$)

With $\alpha = 1$ and no support-excitation, the upright position loses stability for $p_{cri} \approx 1{\cdot}469$ by a supercritical Hopf bifurcation, and the pendulum performs flutter oscillations for $p > p_{cri}$. Figure 7(a) shows the maximum Lyapunov exponent λ_1 versus the load magnitude p with the small initial disturbance: $(0{\cdot}05, -0{\cdot}07, 0{\cdot}0)$. Negative values of λ_1 are seen for $p < p_{cri}$ indicating a static equilibrium, in this case the upright position. For $p > p_{cri}$, λ_1 approximately vanishes which indicates periodic motion. No signs of chaotic dynamics ($\lambda_1 > 0$) appears in Figure 7(a), but for very high load magnitudes ($p > \approx 15$), λ_1 turns positive and the motion will be chaotic.

If strong support-excitation ($v = 2$) is added (Figure 7(b)), the stability of the upright position is increased, as seen also in Figures 2 and 6. The zero solution loses stability for $p_{cri} \approx 3{\cdot}800$ by a subcritical bifurcation, and is replaced by periodic oscillations of the pendulum. For $p > \approx 6{\cdot}5$ positive values of λ_1 are seen, indicating chaotic motion. Figure 7(b) was obtained with the same initial conditions as in Figure 7(a). With a larger initial

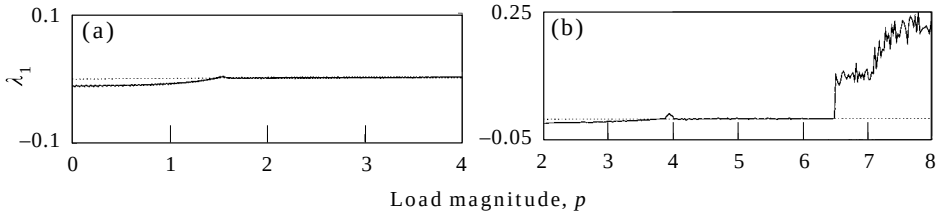

Figure 7. Largest Lyapunov exponent λ_1 plotted versus load magnitude p, (a) $\alpha = 1$, $v = 0$; (b) $\alpha = 1$, $v = 2$; total sampling time 2000 s, transient cut-off 1000 s, sampling frequency 20 Hz. Initial conditions $(0{\cdot}05, -0{\cdot}07, 0, 0)$. Parameter values: $c = 0{\cdot}1$, $\Omega = 50$.

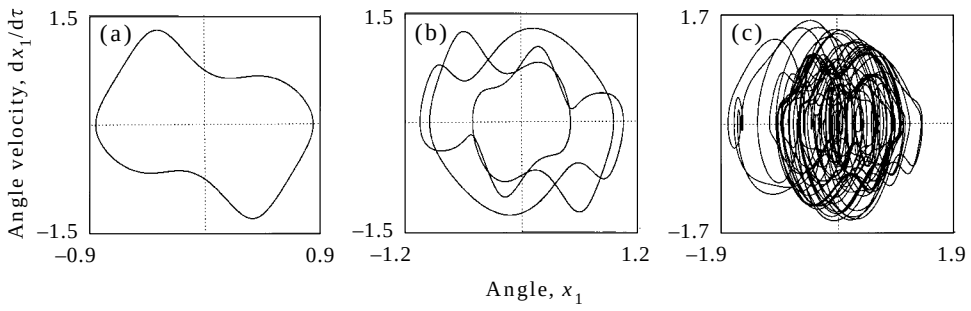

Figure 8. Phase portraits showing lower rod angle velocity $dx_1/d\tau$ versus lower rod angle x_1, based on numerical integration of equations (18) and (19); (a) $p = 3{\cdot}5$, initial conditions (1, 1·5, 0·5, 0·75); (b) $p = 5$; (c) $p = 7$. Parameter values: $c = 0{\cdot}1$, $v = 2$ ($\Omega = 50$). Initial conditions (0·05, −0·07, 0, 0).

disturbance, periodic motion is seen also for values of p slightly less than critical due to the subcritical bifurcation.

More detailed information about the system behaviour for $v = 2$ ($\alpha = 1$) is obtained by using the path-following algorithm PATH. For values of p near the critical value, the bifurcational behaviour can be shown to resemble that of Figure 4(a) for $v = 0{\cdot}5$: i.e., a stable periodic motion exists after a secondary saddle-node bifurcation of the unstable periodic solution. In Figure 8(a) a phase-plot is shown, i.e., a post-transient plot of $dx_1/d\tau$ versus x_1, corresponding to this stable periodic motion. The curve is seen to be distorted due to strong non-linearities, but the motion is still regular. If the load magnitude is increased further, a secondary Hopf bifurcation occurs. This bifurcation results in period-3 motion, as illustrated in Figure 8(b), showing a phase-plot for $p = 5$. If p increases even further, yet another bifurcation occurs, now resulting in chaotic dynamics. Figure 8(c) shows a phase-plot for $p = 7$, showing the post-transient dynamic behaviour. The phase plane is seen to fill out in an unpredicatable way, which suggests chaotic motion (also indicated by $\lambda_1 > 0$, Figure 7(b)).

6.2. THE CASE OF $\alpha = 2$

With $\alpha = 2$, added support-excitation may also significantly change the global non-linear behaviour of the pendulum. For $v = 0$ the bifurcation associated with the divergence instability, occurring for $p_{cri} \approx 3{\cdot}304$, is subcritical. Figures 9(a) and (c) show the largest Lyapunov coefficient plotted versus the load magnitude p, for a weak and a strong initial disturbance, respectively. The upright pendulum position is in both cases replaced by a non-zero static equilibrium when the load is increased beyond the critical level. This is seen as a jumps in λ_1 (λ_1 is still negative). Due to the subcritical bifurcation, the stronger disturbance (Figure 9(c)) pushes the system to the new static equilibrium point also for values of p slightly less than critical. With a further increase in p, the new equilibrium position loses stability by a Hopf bifurcation, leading to chaotic motion ($\lambda_1 > 0$). Numerical simulation reveals that the motion may eventually settle down on a static equilibrium point after an unpredictably long transient period of chaos. Also, a very strong initial disturbance has been shown to may cause the system to settle on large amplitude periodic motion for $p < p_{crit}$, see reference [2].

Figures 9(b) and (d) show λ_1 versus p for added support-excitation, corresponding to $v = 0{\cdot}75$. The figures correspond, like Figures 9(a) and (c) to a weak and a strong initial disturbance. From Figure 9(b) it is seen that the upright pendulum position is now replaced

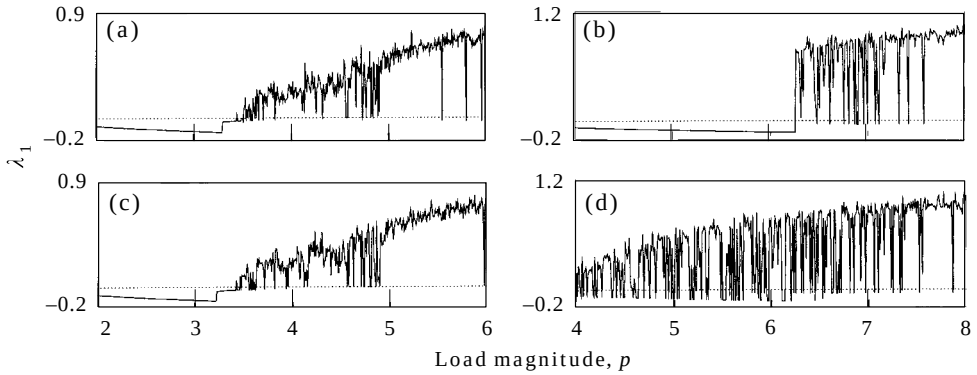

Figure 9. Largest Lyapunov exponent λ_1 plotted versus the load magnitude p; (a) $\alpha = 2$, $v = 0$; (b) $\alpha = 2$, $v = 0{\cdot}75$; (c) $\alpha = 2$, $v = 0$; (d) $\alpha = 2$, $v = 0{\cdot}75$; total sampling time 2000 s, transient cut-off 1000 s, sampling frequency 20 Hz. Initial conditions, (a, b): (0·05, −0·07, 0, 0); (c, d): (1, 1·5, 0·5, 0·75). Parameter values: $c = 0{\cdot}1$, $\Omega = 25$.

directly by chaotic pendulum motion when p is increased beyond the critical level. Actually, chaos appears for load levels less than critical, which shows that even the weak disturbance is sufficient to destabilize the linearly stable upright position. With a stronger initial disturbance, as shown in Figure 9(d), chaos appears far into the pre-critical range, with several narrow "windows" however, where the pendulum settles on a static equilibrium point. As was the case for $v = 0$, the chaotic motion may also for added support-excitation finally settle down on a static equilibrium. However, this happens, if at all, after a long and unpredictable time-range.

For the case of the left and the lower right divergence regions (see e.g., Figure 2), no signs of chaotic behaviour can be traced, with or without excitation of the support. But for the regions studied by examples in this and in the previous section, the results have pointed out that chaotic behaviour of the pendulum is more likely to occur with added support-excitation, compared to the case of a fixed support. Importantly, chaotic dynamics was shown to be possible for load levels less than critical: i.e., even with the upright pendulum position linearly stable.

7. SUMMARY AND CONCLUSIONS

Linear stability and non-linear behaviour of the partially follower-loaded elastic double pendulum with small-amplitude high-frequency (off-resonant) excitation of the support, has been analyzed.

The method of DPM (direct partition of motion) was used to turn the governing model equations into autonomous form, by approximating the added support-excitation by equivalent static forces. Linear stability was investigated and a local non-linear analysis was performed by using the techniques of centre manifold reduction and normal forms, as well as by numerical integration of the original equations and by the use of PATH (a path-following algorithm) applied to the autonomous set of equations. Lyapunov exponents were computed also, in order to study the global behaviour.

The presence of support-excitation has been shown to affect strongly the linear stability of the follower-loaded pendulum. For most values of α, excitation of the support stabilized the system: i.e., a stronger loading is needed to turn the upright position unstable. For a load arrangement corresponding to $\alpha = 1{\cdot}3$, the excitation may, however, destabilize the

system in favour of flutter oscillations. The non-linear behaviour was shown to change, both quantitatively and qualitatively, when support-excitation was added. Supercritical bifurcations were seen to turn into subcritical ones when a sufficient amount of support-excitation was added. This applies to both dynamic and static instabilities, flutter and divergence, respectively. The domain of chaotic dynamics was also seen to increase: e.g., with a pure tangential load ($\alpha = 1$) the pendulum behaves chaotically for moderate load magnitudes when strong support-excitation is applied. Also, for $\alpha = 2$, chaotic dynamics was seen to appear for load levels less than critical, if a large disturbance was applied.

This work has shed light upon possible effects of the interaction between follower-type forces and high-frequency excitation acting upon instability-prone structures. It has been shown that in many cases stability of the original design can be enhanced by the aid of high-frequency excitation, but also that this stability may be sensitive to large disturbances. Also structures subjected to high-frequency excitation are more prone to behave in an unpredictable chaotic manner. However, with this in mind, it is believed by the author that, given considerable future work in this area, high-frequency excitation might be of use when dealing with stabilization of structures.

In this investigation only uni-directional support-excitation was added. Using bi-directional excitation could change the dynamic behaviour of the pendulum, e.g., by changing the stability and positions of static equilibrium points and by altering the basins of attraction for different non-linear solutions. This should be analyzed further. Also, an experimental investigation of this or similar systems is called for.

ACKNOWLEDGMENT

The author wishes to thank Professor I. I. Blekman for suggesting this project and for introducing the method of direct partition of motion to the author.

REFERENCES

1. I. I. Blekhman 1994 *Vibrational Mechanics* (in Russian). Moscow: Fizmalit Publishing Company.
2. J. J. Thomsen 1995 *Journal of Sound and Vibration* **188**, 385–405. Chaotic dynamics of the partially follower-loaded elastic double pendulum.
3. Y. Sugiyama, K. Katayama and S. Kinoi 1995 *Journal of Aerospace Engineering* **8**. Flutter of cantilevered column under rocket thrust.
4. G. Herrmann, S. Nemat-Nasser and S. N. Prasad 1966 *Technical Report no*. 66-4, *National Aeronautics and Space Administration*. Models demonstrating instability of nonconservative mechanical systems.
5. H. Ziegler 1953 *Ingenieur-Archiv* **20**, 49–56. Die Stabilitätskriterien der Elastomechanik.
6. V. V. Bolotin 1963 *Nonconservative Problems of the Theory of Elastic Stability*. Oxford: Pergamon Press.
7. G. Herrmann and I. C. Jong 1966 *Journal of Applied Mechanics* **33**, 125–133. On nonconservative stability problems of elastic systems with slight damping.
8. J. Roorda and S. Nemat-Nasser 1967 *American Institute of Aeronautics and Astronautics* **5**, 1262–1268. An energy method for stability analysis of nonlinear, nonconservative systems.
9. P. L. Kapitza 1951 *Zurnal Eksperimental'noj i Teoreticeskoj Fiziki* **21**, 588–597. Dynamic stability of a pendulum with an oscillating point of suspension (in Russian).
10. G. Erdos and T. Singh 1996 *Journal of Sound and Vibration* **198**, 643–650. Stability of a parametrically excited damped inverted pendulum.
11. I. I. Blekhman and O. Z. Malakhova 1986 *Soviet Physics Doklady* **31**, 229–231. Quasiequilibrium positions of the Chelomei pendulum.
12. J. J. Thomsen 1997 *Vibrations and Stability*: *Order and Chaos*. London: McGraw-Hill.

13. J. S. Jensen 1996 *Proceedings of the EUROMECH 2nd European Nonlinear Oscillation Conference*, *Prague*, Volume **1**, 211–214. Transport of continuous material in vibrating pipes.
14. J. S. Jensen 1997 *Journal of Fluids and Structures* **11**, 327–344. Fluid transport due to nonlinear fluid–structure interaction.
15. E. J. Routh 1960 *Dynamics of Systems of Rigid Bodies. Part II. Articles*. New York: Dover. See pp. 290–301.
16. L. Perko 1991 *Differential Equations and Dynamical Systems*. New York: Springer-Verlag.
17. J. Carr 1981 *Applications of Centre-Manifold Theory*. New York: Springer-Verlag.
18. J. Guckenheimer and P. Holmes 1983 *Nonlinear Oscillations*, *Dynamical Systems*, *and Bifurcations of Vector Fields*. New York: Springer-Verlag.
19. A. H. Nayfeh 1993 *Method of Normal Forms*. New York: Wiley.
20. G. X. Li and M. P. Païdoussis 1994 *International Journal of Non-linear Mechanics* **29**, 83–107. Stability, double degeneracy and chaos in cantilevered pipes conveying fluid.
21. M. P. Païdoussis and C. Semler 1993 *Journal of Fluids and Structures* **7**, 269–298. Nonlinear dynamics of a fluid-conveying cantilevered pipe with an intermediate spring support.
22. C. Kaas-Petersen 1989 *PATH-User's Guide*. England: Department of Applied Mathematical Studies, University of Leeds.
23. A. Wolf, J. B. Swift, H. L. Swinney and J. A. Vastano 1985 *Physica* **16D**, 285–317. Determining Lyapunov exponents from a time series.

APPENDIX

The non-zero components of the vector $\mathbf{b}_{3jkl}$, are,

$$b_{3113} = c, \quad b_{3114} = -\tfrac{3}{4}c, \quad b_{3133} = -\tfrac{1}{2}, \quad b_{3144} = -\tfrac{1}{2}, \quad b_{3223} = c,$$
$$b_{3123} = -2c, \quad b_{3124} = \tfrac{3}{2}c, \quad b_{3224} = -\tfrac{3}{2}c, \quad b_{3233} = \tfrac{1}{2}, \quad b_{3244} = \tfrac{1}{2},$$
$$b_{3111} = \tfrac{1}{12}(12 - 4p + 61v), \quad b_{3222} = -\tfrac{1}{12}(p(3\alpha - 7) + 9 + 29v),$$
$$b_{3112} = \tfrac{1}{4}(4p - 11 - 41v), \quad b_{3122} = \tfrac{1}{4}(p(\alpha - 5) + 10 + 33v), \tag{A1}$$

and of $\mathbf{b}_{4jkl}$ are

$$b_{4113} = -\tfrac{7}{4}c, \quad b_{4114} = \tfrac{5}{4}c, \quad b_{4133} = \tfrac{3}{2}, \quad b_{4144} = \tfrac{1}{2}, \quad b_{4223} = -\tfrac{7}{4}c,$$
$$b_{4123} = \tfrac{7}{2}c, \quad b_{4124} = -\tfrac{5}{2}c, \quad b_{4224} = \tfrac{5}{4}c, \quad b_{4233} = -\tfrac{3}{2}, \quad b_{4244} = -\tfrac{1}{2},$$
$$b_{4111} = \tfrac{7}{12}(p - 3 - 15v), \quad b_{4222} = \tfrac{1}{12}(p(5\alpha - 12) + 15 + 55v),$$
$$b_{4112} = \tfrac{1}{4}(19 - 7p + 75v), \quad b_{4122} = \tfrac{1}{4}(p(8 - \alpha) - 17 - 61v). \tag{A2}$$